J Nanopart Res (2010) 12:1239–1248
DOI 10.1007/s11051-009-9815-7

RESEARCH PAPER

Effect of chain length and electrical charge on properties of ammonium-bearing bisphosphonate-coated superparamagnetic iron oxide nanoparticles: formulation and physicochemical studies

Ali Karimi · Benoit Denizot · François Hindré · Robert Filmon · Jean-Marc Greneche · Sophie Laurent · T. Jean Daou · Sylvie Begin-Colin · Jean-Jacques Le Jeune

Received: 10 April 2009 / Accepted: 17 November 2009 / Published online: 3 December 2009

Abstract Bisphosphonates BP molecules have shown to be efficient for coating superparamagnetic iron oxide particles. In order to clarify the respective roles of electrical charge and the length of the molecules, bisphosphonates with one or two ammonium moieties with an intermediate aliphatic group of 3, 5 or 7 carbons were synthesized and iron oxide nanoparticles coated. The evaluation on their iron core properties was made by transmission electron microscopy (TEM), nuclear magnetic relaxation dispersion (NMRD) profiles and Mössbauer spectra. The core size is close to 5 nm, with a global superparamagnetic behaviour modified by a paramagnetic Fe-based layer, probably due to surface crystal alteration. The hydrodynamic sizes increase slightly with aliphatic chain length (from 9.8 to 18.6 nm). The presence of one or two ammonium group(s) lowers the negative electrophoretic mobility up to bear zero values but reduces their colloidal stability. These BP-coated iron oxide nanoparticles are promising Magnetic Resonance Imaging (MRI) contrast agents.

Keywords Iron oxides · Contrast agents · Superparamagnetic behaviour · Bisphosphonates · NMRD profiles · Mössbauer spectrometry · Colloids · Magnetic Resonance Imaging

Introduction

Iron oxide nanoparticles are used as contrast agents for Magnetic Resonance Imaging (MRI). Most of the

A. Karimi · F. Hindré · J.-J. Le Jeune
Inserm U646, Université d'Angers, 10 rue Bocquel, 49100 Angers, France

B. Denizot (✉)
Centre Hospitalier Annemasse-Bonneville, 64 avenue de Genève, 74130 Bonneville, France
e-mail: BDenizot@chi-annemasse-bonneville.fr

R. Filmon
Service Commun d'Imagerie et d'Analyses Microscopiques, Université d'Angers, rue Haute de Reculée, 49045 Angers Cedex 01, France

J.-M. Greneche
Laboratoire de Physique de l'Etat Condensé UMR 6087, Université du Mans, 72085 Le Mans Cedex, France

S. Laurent
Department of General, Organic and Biochemical Chemistry, NMR and Molecular Imaging Laboratory, University of Mons-Hainaut, Avenue du Champs de Mars 24, 7000 Mons, Belgium

T. J. Daou
Institut de Physique et Chimie des Matériaux de Strasbourg, UMR CNRS-ULP 7504, 23 rue du Loess, BP43, 67034 Strasbourg Cedex 2, France

S. Begin-Colin
Laboratoire de Matériaux à Porosité Contrôlée, UMR CNRS 7016, Université de Haute Alsace, 3 rue Alfred Werner, 68093 Mulhouse Cedex, France

developed agents are powerful enhancers of proton relaxation times, particularly T_2 relaxation times (Weissleder et al. 1995). Amongst the iron oxide particles, the magnetite (Fe_3O_4) and the maghemite (Fe_2O_3) have received much attention during the past two decades because of their ferromagnetic structure and their great technological applicative importance. The magnetite, obtained by coprecipitation of Fe^{3+} and Fe^{2+} salts, has the formula $[Fe^{3+}]_{Td}[Fe^{3+}Fe^{2+}]_{Oh}O_4$, with Td for tetrahedral and Oh for Octahedral sites (Jolivet et al. 2004a, b; Wang et al. 2001). The maghemite, which may be considered as an oxidized form of magnetite, can be described as $[Fe^{3+}]_{Td}[Fe^{3+}_{5/3}L_{1/3}]_{Oh}O_4$ with L for vacancies (Tronc et al. 1998). Owing to mild oxidation conditions, the final iron oxide compositions used in MRI investigations are often reported as intermediate between magnetite (Fe_3O_4) and maghemite (γ-Fe_2O_3), due to the oxidation of the particles during and after synthesis (Daou et al. 2006; Zaitsev et al. 1999).

The small size of the particles (<50 nm) gives rise to single domain particles with superparamagnetic behaviour (instead of ferrimagnetic structure in the case of microcrystalline particles). In medical imaging applications, this property is used in particle contrast agents, with both T_1 and T_2 relaxation time alteration. After intravenous injection, these superparamagnetic colloids should remain for a sufficient length of time in the intravascular compartment: for vascular applications, those particles should avoid (or at least have limited interactions with) the Mononuclear Phagocyte System (MPS) (Groman et al. 1989), a characteristic mainly related to their overall size and their coating. The most common ones are made of biocompatible hydrophilic polymers, such as dextran (Weissleder et al. 1995) or polyethylene glycol (Chapman et al. 2001; Holmlin et al. 2001; Lemarchand et al. 2006; Ostuni et al. 2001; Peracchia et al. 1999). Those polymers reduce the protein adsorption, mainly as high-density polymer brush. The thickness and the density of the polymeric shell can be tuned by changing the nature and the concentration of the monomer, as well as the mean molecular weight (Zaitsev et al. 1999).

Iron oxide cores can also be coated by proteins such as albumin (Peng et al. 2004; Wilhelm et al. 2003) or by small compounds such as dimercaptosuccinic acid (Brillet et al. 2005; Fauconnier et al. 1997; Halbreich et al. 1998) or phosphorylcholine (Ishihara et al. 1998). The interest of the latter molecule is that it contains phosphate groups which are known to allow a strong bonding of the molecules at the surface of nanoparticles (Daou et al. 2008). A disadvantage of phosphorylcholine coating is its pH-dependency which makes these particles not suitable for in vivo biodistribution studies (Denizot et al. 1999). Bisphosphonates BP have been used to overcome this drawback (Portet et al. 2001). BPs are characterized by two phosphonate groups linked to the same carbon or *gem*-structures with the advantage of hydrophilicity and highly anionic electrical charge. Portet et al. (2001) used primary, tertiary and quaternary amine-bearing BPs, in comparison with hydroxyethylenebisphosphonate (HEBP) in biodistribution studies. Primary and tertiary amines induce high particle capture rate by MPS. The quaternary amine-bearing BP, 6-ammonium-3-oxo-5-hydroxybisphosphonate, was interesting because of the relatively slow clearance of the particles in the blood (27 min of vascular half-life in the rat).

Others teams (Lalatonne et al. 2008; Port et al. 2004) also used bisphosphonates for the coating of their iron oxide nanoparticles for the MRI or for coupling fluorescence markers.

Our main goal is to obtain 'stealth' particles (with low recognition by MPS system) by coating particles by several quaternary-ammonium BPs. In order to keep the hydrophilic effects and improve the particle size distribution, two aspects were evaluated:

- The length of methylenes (3, 5 or 7) between the ammonium and bisphosphonates groups.
- The particle electrical charge of the bisphosphonate bearing one or two ammonium groups (Fig. 1).

Iron oxide nanoparticles were coated with these bisphosphonates. We report here the results of the physicochemical studies by the nuclei of the nanoparticles [Transmission electron microscopic (TEM), nuclear magnetic resonance dispersion NMRD profiles, ^{57}Fe Mössbauer spectrometry and relaxometry] and the coating effect (hydrodynamic size, electrophoretic mobility).

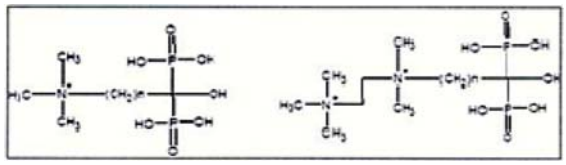

Fig. 1 Molecules scheme of synthetized bisphosphonates bearing one or two ammonium groups (with $n = 3, 5, 7$)

Experimental

Preparation

Chemistry

HEBP or 1-hydroxyethylidene bisphosphonic acid (Sigma) (also known as HEDP or 1-hydroxyethylidene diphosphonic acid) is used without further purification.

Trialkylammonioalkylbisphosphonates (N^+C_nBP) are constituted by a trimethylammonium group at one side and bisphosphonates at the other side. Between those functions, three sizes of methylene groups are studied: 3, 5 or 7. In order to keep the hydrophilicity of the molecules, the limit is 7.

Diammonioalkylbisphosphonates ($2N^+C_nBP$) are constituted by two ammonium groups separated by ethylene groups at one side and the bisphosphonates groups at the other side. Between those two functions, there are n (3 or 5) methylene groups.

All synthetized compounds were analysed by ^1H and ^{31}P NMR in D_2O with a JEOL GSX apparatus.

Synthesis of trialkylammonioalkylbisphosphonates (N^+C_nBP) First, the formation of the monoammonium acid is obtained by the substitution of the trimethylamine (Sigma) to a bromoacid (Sigma) with a ratio of 10:1 in acetonitrile.

The formation of bisphosphonate needs two steps: first, the formation of the acid chloride from the previous obtained compound with two equivalents of thionyle chloride, $SOCl_2$ (Sigma) and then followed, at 5°C, by the addition of two equivalents of tris(triméthylsilyl)phosphate $P(OSiMe_3)_3$ (Sigma) to form the bisphosphonates.

Example for $n = 3$:

^1H NMR (D_2O) for $n = 3$: $\delta = 3.7$ (t, 2H, N^+–CH_2), 3.2 (s, 9H, –$N(CH_3)_3$), 2 (t, 2H, –CH_2–$C(OH)(PO_3H_2)_2$), 1.6 (t, 2H, –CH_2–CH_2–N^+).
^{31}P NMR (D_2O): $\delta = 20$ ppm.

Synthesis of diammonium bisphosphonates ($2N^+C_n$ BP) The bromoacid reacted with the thionyle chloride and then with two equivalents of triethylphosphite $P(OEt)_3$ (Sigma) to obtain the bisphosphonate.

A reaction of methylation is made with the iodomethane CH_3I (Sigma) to the tetramethylethylenediamine which led to the 2-(dimethylamino)-*N*,*N*,*N*-trimethylethanaminium.

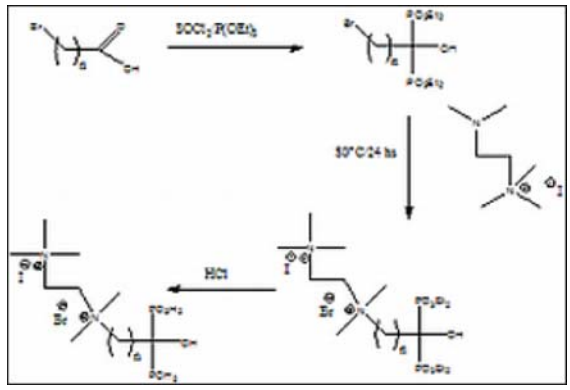

Fig. 2 Scheme reaction for the formation of the diammonium bisphosphonates

Then, the following step (Fig. 2) is the substitution of the bromobisphosphonate with the 2-(dimethylamino)-*N*,*N*,*N*-trimethylethanaminium at 80°C during 24 h.

Example for $n = 3$:

^1H NMR (D_2O): $\delta = 3.6$ (t, 2H, N^+–CH_2), 3.4 (m, 2H, $^+N(CH_3)_2$–CH_2–$(CH_2)_2$), 3.2 (t, 9H, $^+N(CH_3)_3$), 3 (t, 2H, $^+N(CH_3)_2$–CH_2–CH2–N^+ $(CH_3)_3$), 2.2 (s, 2H, –CH_2–$C(OH)(PO_3H_2)_2$), 1.5 (m, 2H, –CH2–CH2–$C(OH)(PO_3H_2)_2$)
^{31}P NMR (D_2O): $\delta = 20$ ppm.

Formulation of iron oxide nanoparticles

The iron oxide was prepared by coprecipitation of iron salts (Fe^{2+} and Fe^{3+}) by a down-scaled method derived from Babes et al. (1999).

Mix of 100 µl of ferric ions $FeCl_3 \cdot 6H_2O$ (0.67 mol l^{-1}) with 100 µl of ferrous ions $FeCl_2 \cdot 4H_2O$ (0.31 mol l^{-1}) in a solution of 2 ml of tetramethylammonium hydroxide $TMAOH \cdot 5H_2O$ (1 mol l^{-1}) by a peristaltic pump injection (Millipore, France) under vigorous magnetic agitation at room temperature which leads to a black suspension. After waiting for 2 min, 480 µl of the bisphosphonates at 0.1 mol l^{-1} are injected. After 5 min of vigourous stirring, 600 µl of TES (N-[Tris(hydroxymethyl)methyl]-2-aminoethanesulfonic acid)-hydrochloric acid (Sigma) are added. After 15 min of stirring, the solution is deposited in a Biogel P6 column (Biorad). The solution is taken out by a constant debit (0.3 ml mn^{-1}) with a peristaltic pump.

All the black fractions are collected and filtered through a 0.2 μm filter.

Water used for all these experiments is injectable grade water (Cooper, France).

Experimental techniques

Studies on iron oxide nanoparticle cores

Iron concentration The solution of iron oxide is diluted at 1/10 with HCl 30% for 2 h at room temperature. Then, the solution becomes yellow, characteristic of iron ions in concentrate HCl. Dilution at 1/10 of the former solution in injectable grade water allows the evaluation of iron concentration by spectrophotometry method at 340 nm. This method of colorimetric determination of concentrations was used by Pouliquen (1988).

Transmission electron microscopy A drop of coated nanoparticle suspension is deposited on a copper grid of 3-mm diameter (previously recovered with a celloïdine film) and observed with a JEOL 2011 apparatus (France), with an acceleration tension of 140 kV and a magnification of 100,000.

Magnetic relaxivity The iron oxide nanoparticle suspensions are diluted with four different concentrations in water. The T_1 and T_2 relaxation times are measured in milliseconds at 4–5°C and 20 MHz with a Minispec Bruker spectrometer (Wissembourg, France). T_1 relaxometry is estimated by inversion-recovery sequences, and T_2 relaxometry is determined by CPMG sequences. The relaxivity of the particles r_1 and r_2 corresponds to the slopes of the curves of the inverse relaxation times as a function of iron concentration. In all experiments, the linear correlation coefficient of the curve fit is 0.99.

Magnetic relaxivities at 20 and 60 MHz were measured with the Minispec PC 120 and 60, respectively.

Two different temperatures, low (4–5°C) and higher (37°C), were studied for the different coatings of nanoparticles.

NMRD profiles The NMRD Profiles are recorded at 37°C on a Fast Field Cycling Relaxometer (Stelar, Mede, Italy). The longitudinal relaxivities (r_1), which characterize the increase of relaxation rate of water protons per millimole of iron per litre, are measured over a magnetic field range from 0.24 mT to 2.4 T. The fitting of the experimental points gives two principal properties of iron oxide core: their specific magnetization and their core size.

Mössbauer spectrometry ^{57}Fe Mössbauer spectra are recorded at 300 and 77 K on a conventional constant acceleration transmission spectrometer with a ^{57}Co(Rh) source. The spectra are fitted by means of the MOSFIT program.

Owing to the high amount of the particles needed for this test, a 50 ml formulation method is used (Denizot et al. 1999). The nanoparticles are coated by the monoammonium bisphosphonates (N^+C_5BP). Suspensions are then dialysed for 2 h against distilled water and lyophilized to obtain a black powder.

Studies on nanoparticle coatings

Hydrodynamic particle size The hydrodynamic particle sizes are measured by photon correlation spectroscopy technique at 90° with an Autosizer 4700 (Malvern Instruments, France) and Autocontin fitting method. Samples, at pH = 7, are filtered using a 0.2 μm Minisart® (Sartorius, France) filter before measurement.

Electrophoretic mobility The electrophoretic mobility of the different nanoparticles is measured with a Zetasizer 2000 (Malvern Instruments, France) at pH 7 with injectable grade water.

The influence of pH is evaluated with a Malvern Zetasizer (Nano-ZS) in 10^{-1} mol l^{-1} $NaClO_4$ solution. The colloidal suspensions at pH 7 are acidified with HCl to get the zeta potential for pH lower than 7 and are basified with NaOH for upper pH. The zeta potential was calculated from the electrophoretic mobility after the Hückel law which takes into account the fact that the radius of the particles is small by comparison with the thickness of the electric double layer.

Results

The results concern the coating of nanoparticles by three kinds of BPs: HEBP, trialkylammonioalkylbisphosphonates, N^+C_nBP, ($n = 3$, 5 and 7) and diammonium bisphosphonates, $2N^+C_nBP$ ($n = 3$, 5).

Studies on iron oxide nanoparticle cores

Iron nuclei

The results are listed in Table 1. The final suspension iron concentration is quite similar for the coating of nanoparticles by the HEBP and the monoammonium alkyl bisphosphonates. For the coating by the diammoniumalkyl bisphosphonates, the iron concentration is roughly decreased by half. The difference of concentrations is due to the coating. Indeed, the coating with $2N^+C_nBP$ leads to a zero potential charge, probably leading to colloidal instability. Therefore, the concentration of nanoparticles with $2N^+C_nBP$ is less important than with N^+C_nBP, which is translated by this decrease of the iron oxide concentrations.

Transmission electron microscopy

As shown in Fig. 3, the mean particle core is estimated at around 5.0 ± 1.5 nm with a rather narrow size distribution.

Magnetic relaxivity

The coating of the iron oxide cores by the N^+C_nBP reveals the increase of the r_2, as the number of carbon increases (Table 1).The presence of aggregation is suspected.

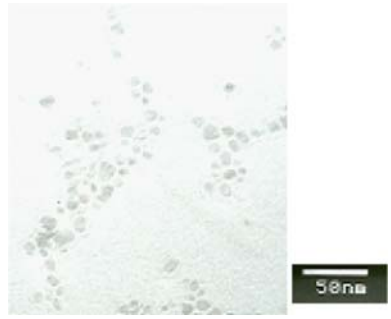

Fig. 3 TEM of the as-prepared iron oxide particles

By comparison with monoammonioalkyl bisphosphonate, and for the same number of methylene groups, the relaxivities r_1 of diammonioalkylbisphosphonates are quite close. Nevertheless, the r_2 is increased with probable presence of aggregates.

Two temperatures were studied: 4–5°C and 37°C. The aim was to study the effect of different bisphosphonate coatings on the iron oxide nanoparticles.

If the r_2 relaxivity is constant for 20 and 60 MHz at 37°C, this is not the case for the r_1 relaxivity. Indeed, Table 2 shows the decrease of the r_1 relaxivity from 20 to 60 MHz, at 37°C and 4–5°C, respectively.

For a constant applied field, the temperature effect was studied. Indeed, from 4–5 to 37°C, the r_1 relaxivity diminishes, especially for the 20 MHz. Then the temperature has an influence on the relaxivity, therefore, on the diffusion of water

Table 1 Iron concentration, hydrodynamic sizes, specific magnetization, radius of the particles by fitting of NMRD curves at 37°C and zeta potentials for the different coatings

Nanoparticles coated by	Final iron concentration ($g\ l^{-1}$)	Hydrodynamic size (nm)	Specific magnetization ($A\ m^2\ kg^{-1}$)	NMRD derived size (nm)	Zeta potential (mV)
HEBP	0.96 ± 0.23	15.00 ± 1.50 PI = 0.40	50	4.44	−30
N^+C_3BP	0.74 ± 0.30	9.80 ± 1.50 PI = 0.27	34	4.75	−23
N^+C_5BP	0.80 ± 0.18	12.50 ± 1.00 PI = 0.34	42	4.36	NA
N^+C_7BP	0.88 ± 0.30	18.60 ± 1.50 PI = 0.50	36	5.12	NA
$2N^+C_3BP$	0.36 ± 0.03	NA	NA	NA	NA
$2N^+C_5BP$	0.43 ± 0.23	23.00 ± 3.00 PI = 0.35	41	4.80	0

NA Not available; *PI* polydispersity index

Table 2 Relaxivities r_1 and r_2 (s^{-1} mM^{-1}) at 20 and 60 MHz at 37 and 4–5°C

Particles coated by	r_1 at 20 MHz, at 4°C	r_2 at 20 MHz, at 4°C	r_2/r_1 at 20 MHz, at 4°C	r_1 at 20 MHz, at 37°C	r_2 at 20 MHz, at 37°C	r_1 at 60 MHz, at 5°C	r_1 at 60 MHz, at 37°C	r_2 at 60 MHz, at 37°C
HEBP	34.60 ± 5.07	99.85 ± 8.21	2.96 ± 0.64	22.08	46.39	12.20	13.92	42.17
N^+C_3BP	21.55 ± 5.59	56.75 ± 12.80	2.52 ± 0.11	10.65	20.10	7.24	7.16	18.44
N^+C_5BP	23.35 ± 3.89	68.58 ± 17.19	2.96 ± 0.75	15.48	30.19	8.10	9.68	29.32
N^+C_7BP	21.47 ± 5.21	68.09 ± 10.39	3.27 ± 0.63	12.35	23.87	4.91	5.95	18.29
$2N^+C_3BP$	16.77 ± 2.55	45.83 ± 5.46	2.80 ± 0.74	6.86	27.25	2.24	3.15	27.97
$2N^+C_5BP$	24.72 ± 3.65	106.26 ± 7.30	4.35 ± 0.56	16.61	39.62	8.70	9.42	37.36

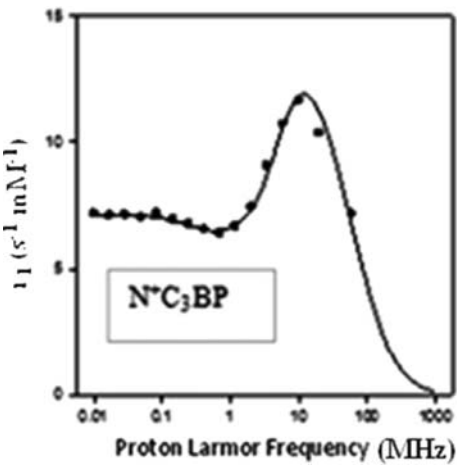

Fig. 4 NMRD curve particles coated by N^+C_3BP

molecules. Therefore, at low temperature (4–5°C), this movement is slowed down, thus increasing the relaxivity, due to a longer translation correlation time of the water protons close to the iron oxide.

NMRD profiles

All the NMRD profiles (similar to Fig. 4) have the same shape: the first part is a plateau at low-field intensity after which the curves increase, and a hump appears. The third part is the decrease in the relaxivity up to zero. This shape of NMRD curves can perfectly be explained by the outer sphere model adapted to a suspension of superparamagnetic particles as described before by Roch et al. (1999). At low field, the relativity is decreased because of the shortening of the correlation time by the Néel relaxation component. A small dispersion at low field attests of a low anisotropy energy (which is characteristic of USPIO particles and probably due to a presence of few aggregated particles). Indeed, a part of the magnetization of the superparamagnetic crystal is then free to precess. At high field, the magnetization of the superparamagnetic crystal is locked to external field direction and the correlation time of the outer sphere theory takes, therefore, into account only the diffusion correlation time. The high field dispersion allows, therefore, for the determination of the crystal size and the specific magnetization. In conclusion, the presence of a peak is due to the evolution of the Curie relaxation component which increases with the magnetic field value.

The theoretical model (solid line—according to the Eq. 31 of the article of Roch et al. 1999) is close to the experimental points, which is concordant with the superparamagnetic behaviour of the iron oxide particles.

Table 1 indicates the calculated core sizes between 4 and 5.12 nm derived from curves. These values are similar to TEM ones. The specific magnetization of the particles is around 50 A m^2 kg^{-1} for HEBP-coated particles and around 40 A m^2 kg^{-1} for the other ones. This is clearly lower than well-structured micrometre-sized magnetite which has a specific magnetization close to 92 A m^2 kg^{-1} (Zaitsev et al. 1999), the maghemite ones being around 56 A m^2 kg^{-1}.

Mössbauer spectrometry

The Mössbauer spectra recorded at 300 and 77 K on the as-prepared particles are illustrated in Fig. 5. One observes at 300 K, a quadrupolar doublet with very broad lines and at 77 K, a sextet composed of asymmetrical and broadened lines. Such hyperfine

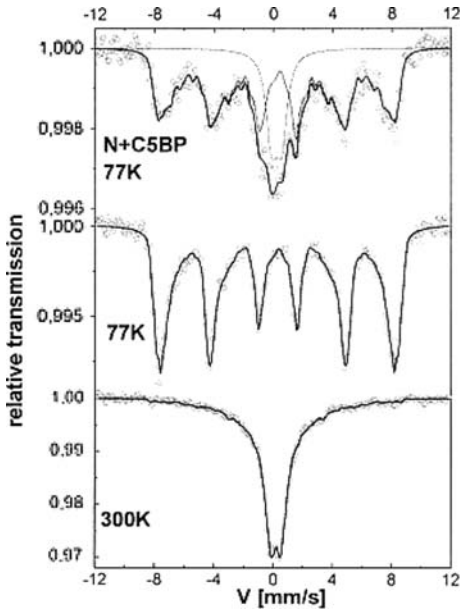

Fig. 5 300 and 77 K Mössbauer spectra of particle cores before coating (*bottom* and *middle*); 77 K Mössbauer spectrum of the ferrofluid resulting from the particles coated by N^+C_5BP at 77 K (*top*)

structures strongly differ from those observed on microcrystalline magnetite or maghemite phases because of the presence of superparamagnetic fluctuations. According to the shape of spectra, one can conclude the presence of non-interacting superparamagnetic nanoparticles probably composed of magnetite and maghemite resulting from partial oxidation.

In the case of the coated nanoparticles by N^+C_5BP, only the spectrum was recorded at 77 K on the frozen system because of the low f factor which is characteristic of the ferrofluid sample observed at room temperature. The spectrum can be seen as the superposition of two components: a quadrupolar feature and a magnetic sextet which fairly compares to that observed at 77 K on the non-coated nanoparticles. In addition, the application of an (small) external magnetic field gives rise to a spectrum also composed of two components with the same proportions and where only the magnetic sextet reveals less broadened lines, due to a lowering of superparamagnetic fluctuations. Consequently, the two components are assigned to the presence of a paramagnetic layer at the surface of the coated particles and their core, respectively (Daou et al. 2007). The present coated nanoparticles can be, thus, described as nanocomposites with a ferric oxide core; a paramagnetic interface layer resulting from a ferric phosphate oxide phase and the superficial bisphosphonate molecules: indeed, the isomer shift value clearly indicates the presence of Fe^{3+} ions in octahedral sites, allowing the conclusion that phosphatation originates an iron-phosphate complex. As the absorption areas are estimated at 80:20% for magnetic and paramagnetic components, respectively, and as the radius of the non-coated particles is around 5 nm, the mean thickness of the paramagnetic layer corresponds to about two atomic layers.

Concerning the coating of the nanoparticles

Hydrodynamic particle size The increasing of methylene groups leads to an increase of hydrodynamic diameter, as shown the Table 1. However, the presence of two methylene groups cannot increase the size of the particles from 9.8 nm for those coated with N^+C_3BP to 12.5 nm for those coated with N^+C_5BP. The size obtained is also due to the presence of few microscopic aggregates particles revealed by the polydispersity index. For the nanoparticles coated with N^+C_3BP, this index (0.27) is the lowest, which means that the aggregation of particles are fewer than the others coatings. The remarks of the polydispersity index can be made for the others coating, especially for N^+C_7BP, which this index (0.50) is the highest. This result can explain the rough variation of size between the particles coated with N^+C_7BP (18.60 nm) compared with N^+C_5BP (12.50 nm). One can note the increasing of number of methylene groups leads also to an increase of the polydispersity index. The problem could be a question of solubility of the coating molecules with the solvent used which is water, with a partial hydrophobic effect between coated particles. For $2N^+C_5BP$, the presence of two quaternary amines gives a good solubility of the coated molecules with water; therefore, the polydispersity index is low enough (0.35).

Zeta potential Table 1, right column, shows the particles zeta potentials according to the coating. The presence of the charge (due to the quaternary group of the coating) induces a progressive neutralization of

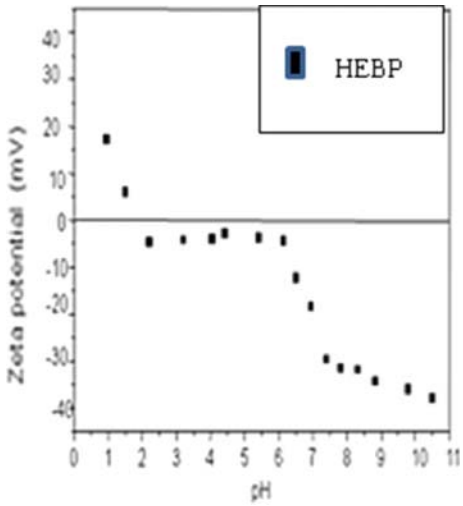

Fig. 6 Zeta potential evolution of HEBP-coated iron oxide nanoparticles as a function of pH

the negative electrical charge due to bound bisphosphonate molecules.

Figure 6 shows the effect of the pH on the zeta potential for the magnetite nanoparticles coated with HEBP in 100 mM $NaClO_4$ solution. The isoelectric point (iep) of the uncoated magnetite is usually found to be around 7 (Daou et al. 2007; Illés and Tombacz 2004; Jolivet et al. 2004a, b; Kosmulski 2004; Peng et al. 2004). In our case, the iep value of those HEBP-coated particles is around 2, with a probable degradation of particle structure at this highly acid pH. Nevertheless, a shift of the zeta potential curve towards acid pH is observed confirming the coating of the surface of the nanoparticles by the HEBP molecules. Such a shift has already been observed during the fixation of orthophosphoric acid on iron oxide nanoparticles (Daou et al. 2007).

Discussion

New quaternary amine bisphosphonate compounds were synthesized in order to coat iron oxide nanoparticles.

Two aspects have been considered on coated suspension properties:

- The effect of the length of methylene groups
- The effect of the number of ammonium groups

The formulation by coprecipitation is a classical way to obtain the iron oxide particles (Babes et al. 1999; Denizot et al. 1999; Peng et al. 2004; Portet et al. 2001). As Jolivet (1994) noted, some parameters, such as pH, the ionic force of the medium, influence the size of the particles. Our preparation method, derived from Babes et al. (1999), leads to small stable nanoparticles (iron cores around 5 nm by TEM, in accordance with NMRD derived data) which are looked upon as superparamagnetic in NMRD (Laurent et al. 2004; Roch et al. 1999) and Mössbauer experiments. Even if the relatively low saturation aimantation estimated by NMRD experiments (lower than 51 A m^2 kg^{-1}) does not allow a differentiation between maghemite and magnetite (or a mix of both), Mössbauer spectra of bare cores are in favour of magnetite presence, with an added paramagnetic layer for BP-coated particles. This is compatible with a superficial layer of about two layers of iron atoms. Another team (Zaitsev et al. 1999) synthesized iron oxide particles by using the TMAOH base, leading to a stable colloid solution. In the Mössbauer spectra of his bare particles, the paramagnetic peak area was 16% of the total area at room temperature. This is not very far from our results, with a paramagnetic layer only induced by the BP fixation on the particles. One explanation for the slight difference may be based on the size of the particles. In our case, the mean size of the bare particles is around 5 nm, whereas in Zaitsev's study, it is between 40 and 50 nm.

As shown in Table 1, the length of the bisphosphonates coating the particles induces a variation of hydrodynamic sizes of the contrast agents. The longer the aliphatic chain is, the bigger the final particle size from 9.8 to 18.6 nm for the N^+C_nBP (n from 3 to 7). Owing to the limited molecular length increase (around 0.5 nm) between N^+C_3BP and N^+C_7BP molecules, the explanation of this large shift in particle size is probably due to search in particle aggregation—revealed by the polydispersity index—as well as the large value of $2N^+C_5BP$-coated particles. Globally, there is a similar tendency between hydrodynamic size and r_2/r_1 ratio (Table 2), which is known to be very sensitive to particle size but also aggregation state. Despite a purification of particles by column, some particles aggregate. The question is whether the onset of this aggregation appears during the formulation step or after recovering where few particles slowly aggregate. In order to

reduce this aggregation phenomenon in negative surface charge, it would be interesting to replace some charged molecules by neutral molecules, as Whiteside's studies (Ostuni et al. 2001). In a practical aspect, it may be delicate to control the surface mixture because the coating on the nanoparticles is not always homogeneous due to self aggregation molecules. Nevertheless, incorporating of small neutral molecules with charged ones could be one way to improve the stability of nanoparticles.

About the electric surface charge, the zeta potential of the three kinds of coating shows the effect of 0, 1 or 2 groups of ammoniums bearing the bisphosphonates. The presence of ammonium groups lowers the negative electrophoretic mobility of BP-coated nanoparticles, giving a neutral charge for the $2N^{+}C_{n}BP$ particles. Owing to this low electrical charge, the absence of interparticle electrical repulsion should be considered to explain the low colloidal stability of $2N^{+}C_{5}BP$-coated nanoparticles. This aspect of aggregation was also underlined in the relaxometry's studies. The advantage of coating by $N^{+}C_{n}BP$ is the more negative surface charge, reducing the aggregation aspect compare to others coating. In this case, the presence of trimethylamine groups on the outer side of the particles with positive charges leads to a minimum repulsion of the particles, whatever the pH is. That is the main advantage of this choice of a quaternary amine group. However, the presence of two positive charges, due to the two quaternary amine groups in $2N^{+}C_{n}BP$, is compensated with the two negative charges of the bisphosphonates coating the nanoparticles, leading to a neutral charge. As far as the mechanism of fixation of bisphosphonates with nanoparticles is concerned, those results are in accordance with ATR-FTIR of Lalatonne's study (Lalatonne et al. 2008).

Conclusion

Small-sized (5 nm) iron oxide nanoparticles were coated by BPs bearing zero, one or two ammonium groups. The large discrepancy between core and hydrodynamic sizes is attributed to limited interparticle aggregation, as is the tendency to larger sizes by longest and ammonium-bearing coating molecules.

Despite their limited colloidal stability, these BP-coated nanoparticles are interesting tools which enable us to understand the effects of global electrical charge and coating thickness in in vivo biodistribution experiments for very small hard-core objects of a size comparable to medium-sized proteins.

Biodistribution studies are in progress to assess the potentialities of these particles as MRI contrast agents.

Acknowledgements Financial support provided by 'Collectivités territoriales' of Angers is gratefully acknowledged. The work of NMRD profiles was supported by the FNRS and the ARC Program 05/10-335 of the French Community of Belgium. The support and sponsorship concerted by COST Action D38 and the EMIL project are kindly acknowledged.

References

Babes L, Denizot B, Tanguy G, Le Jeune JJ, Jallet P (1999) Synthesis of iron oxide nanoparticles used as MRI contrast agents: a parametric study. J Colloid Interface Sci 212:474–482

Brillet PY, Gazeau F, Luciani A, Bessoud B, Cuénod CA, Siauve N, Pons JN, Poupon J, Clément O (2005) Evaluation of tumoral enhancement by superparamagnetic iron oxide particles: comparative studies with ferumoxtran and anionic iron oxide nanoparticles. Eur Radiol 15:1369–1377

Chapman RG, Ostuni E, Liang MN, Meluleni G, Kim E, Yan L, Pier G, Warren HS, Whitesides GM (2001) Polymeric thin films that resist the adsorption of proteins and the adhesion of bacteria. Langmuir 17:1225–1233

Daou TJ, Pourroy G, Begin-Colin S, Grenèche JM, Ulhaq-Bouillet C, Legaré P, Bernhardt P, Leuvrey C, Rogez G (2006) Hydrothermal synthesis of monodisperse magnetite nanoparticles. Chem Mater 18:4399–4404

Daou TJ, Begin-Colin S, Grenèche JM, Thomas F, Derory A, Bernhardt P, Legaré P, Pourroy G (2007) Phosphate adsorption properties of magnetite-based nanoparticles. Chem Mater 19:4494–4505

Daou TJ, Grenèche JM, Pourroy G, Buathong S, Derory A, Ulhaq-Bouillet C, Donnio B, Guillon D, Begin-Colin S (2008) Coupling agent effect on magnetic properties of functionalized magnetite-based nanoparticles. Chem Mater 20:5869–5875

Denizot B, Tanguy G, Hindré F, Rump E, Le Jeune JJ, Jallet P (1999) Phosphorylcholine coating of iron oxide nanoparticles. J Colloid Interface Sci 209:66–71

Fauconnier N, Pons JN, Roger J, Bee A (1997) Thiolation of maghemite nanoparticles by dimercaptosuccinic acid. J Colloid Interface Sci 194:427–433

Groman EV, Josephson L, Lewis JM (1989) Biologically degradable superparamagnetic materials for use in clinical applications. US Patent 4,827,945

Halbreich A, Roger J, Pons JN, Geldwerth D, Da Silva MF, Roudier M, Bacri JC (1998) Biomedical applications of maghemite ferrofluid. Biochimie 80:379–390

Holmlin RE, Chen X, Chapman RG, Takayama S, Whitesides GM (2001) Zwitterionic SAMs that resist non-specific adsorption of protein from aqueous buffer. Langmuir 17:2841–2850

Illés E, Tombacz E (2004) The role of variable surface charge and surface complexation in the adsorption of humic acid on magnetite. Colloids Surf A 230:99–109

Ishihara K, Nomura H, Mihara T, Kurita K, Iwasaki Y, Nakabayashi N (1998) Why do phospholipid polymers reduce protein adsorption? J Biomed Mater Res 39:323–330

Jolivet JP (1994) De la solution à l'oxyde. CNRS Editions, Paris

Jolivet JP, Chanéac C, Tronc E (2004a) Iron oxide chemistry. From molecular clusters to extended solid networks. Chem Commun 5:481–487

Jolivet JP, Froidefond C, Pottier A, Chanéac C, Cassaignon S, Tronc E, Euzen P (2004b) Size tailoring of oxide nanoparticles by precipitation in aqueous medium. A semi-quantitative modeling. J Mater Chem 14:3281–3288

Kosmulski M (2004) pH-dependent surface charging and points of zero charge II. J Colloid Interface Sci 275:214–224

Lalatonne Y, Paris C, Serfaty JM, Weinmann P, Lecouvey M, Motte L (2008) Bis-phosphonates-ultra small superparamagnetic iron oxide nanoparticles: a platform towards diagnosis and therapy. Chem Commun 2553–2555

Laurent S, Nicotra C, Gossuin Y, Roch A, Ouakssim A, Vander Elst L, Cornant M, Soleil P, Muller RN (2004) Influence of the length of the coating molecules on the nuclear magnetic relaxivity of superparamagnetic colloids. Phys Status Solidi 1:3644–3650

Lemarchand C, Gref R, Passirani C, Garcion E, Petri B, Müller R, Costantini D, Couvreur P (2006) Influence of polysaccharide coating on the interactions of nanoparticles with biological systems. Biomaterials 27:108–118

Ostuni E, Chapman RG, Holmlin RE, Takayama S, Whitesides GM (2001) A survey of structure–property relationships of surfaces that resist the adsorption of protein. Langmuir 17:5605–5620

Peng ZG, Hidajat K, Uddin MS (2004) Adsorption of bovine serum albumin on nanosized magnetic particles. J Colloid Interface Sci 271:277–283

Peracchia MT, Harnisch S, Pinto-Alphandry H, Gulik A, Dedieu JC, Desmaële D, d'Angelo J, Müller RH, Couvreur P (1999) Visualization of in vitro protein-rejecting properties of PEGylated stealth® polycyanoacrylate nanoparticles. Biomaterials 20:1269–1275

Port M, Corot C, Raynal I, Rousseaux O (2004) Nouvelles compositions de particules magnétiques recouvertes de dérivés gem-bisphosphonates. FR patent FR 2848850

Portet D, Denizot B, Rump E, Le Jeune JJ, Jallet P (2001) Nonpolymeric coatings of iron oxide colloids for biological use as magnetic resonance imaging contrast agents. J Colloid Interface Sci 238:37–42

Pouliquen D (1988) Conception et évaluation de produits de contraste pour l'IRM du proton. PhD thesis

Roch A, Muller RN, Gillis P (1999) Theory of proton relaxation induced by superparamagnetic particles. J Chem Phys 110:5403–5411

Tronc E, Chanéac C, Jolivet JP (1998) Structural and magnetic characterization of ε-Fe_2O_3. J Solid State Chem 139:93–104

Wang YXJ, Hussain SM, Krestin GP (2001) Superparamagnetic iron oxide contrast agents: physicochemical characteristics and applications in MR imaging. Eur Radiol 11:2319–2331

Weissleder R, Bogdanov A, Neuwelt EA, Papisov M (1995) Long-circulating iron oxides for MR imaging. Adv Drug Deliv Rev 16:321–334

Wilhelm C, Billotey C, Roger J, Pons JN, Bacri JC, Gazeau F (2003) Intracellular uptake of anionic superparamagnetic nanoparticles as a function of their surface coating. Biomaterials 24:1001–1011

Zaitsev VS, Filimonov DS, Presnyakov IA, Gambino RJ, Chu B (1999) Physical and chemical properties of magnetite and magnetite-polymer nanoparticles and their colloidal dispersions. J Colloid Interface Sci 212:49–57